

Spectuner: A Framework for Automated Line Identification of Interstellar Molecules

YISHENG QIU ,¹ TIANWEI ZHANG ,^{1,2} THOMAS MÖLLER ,² XUE-JIAN JIANG ,¹ ZIHAO SONG,¹ HUAXI CHEN,¹ AND DONGHUI QUAN¹

¹Research Center for Astronomical computing, Zhejiang Laboratory, Hangzhou, China

²I. Physikalisches Institut, Universität zu Köln, Zülpicher Straße 77, 50937 Köln, Germany

ABSTRACT

Interstellar molecules, which play an important role in astrochemistry, are identified using observed spectral lines. Despite the advent of spectral analysis tools in the past decade, the identification of spectral lines remains a tedious task that requires extensive manual intervention, preventing us from fully exploiting the vast amounts of data generated by large facilities such as ALMA. This study aims to address the aforementioned issue by developing a framework of automated line identification. We introduce a robust spectral fitting technique applicable for spectral line identification with minimal human supervision. Our method is assessed using published data from five line surveys of hot cores, including W51, Orion-KL, Sgr B2(M), and Sgr B2(N). By comparing the identified lines, our algorithm achieves a recall of $\sim 84\% - 98\%$. Our code, named SPECTUNER, is publicly available on GitHub.

1. INTRODUCTION

Interstellar molecules, crucial for probing chemical and physical processes in the interstellar medium, are identified through their spectral lines. Current and future facilities, e.g. IRAM, ALMA, NOEMA, ng-VLA, and SKA, generate a vast amount of spectral line data annually. Analyzing the data presents a significant challenge.

In the past decade, many tools have been developed to analyze and identify molecular spectral lines, including WEEDS (Maret et al. 2011), CASSIS (Vastel et al. 2015), XCLASS (Möller et al. 2017), MADCUBA (Martín et al. 2019), and PYSPECKIT (Ginsburg et al. 2022). Most of these tools treat spectral line identification as a curve fitting problem. In practice, spectral line identification involves excessive manual processes, including selecting molecules, making initial guesses for fitting, and checking the goodness of fit, which make spectral line identification a laborious task.

The main goal of this study is to develop an automated line identification framework of interstellar species. Our algorithm, which builds on XCLASS (Möller et al. 2017), can automatically analyze an observed single-pointing spectrum and produce the best-fitting spectrum, asso-

ciated parameters, and a table of identified lines with minor human intervention. Our algorithm is assessed using published line survey data of hot cores towards W51, Orion KL, Sgr B2(M) and Sgr B2(N). Our tool, named SPECTUNER, is publicly available on GitHub¹.

This paper is structured as follows. Section 2 describes our methodology. The line survey data used for evaluating our algorithm are introduced in Section 3. Our results are presented in Section 4. Finally, this work is summarized in Section 5.

2. METHODOLOGY

2.1. Overview

Figure 1 demonstrates the flowchart of our proposed framework for automated line identification. The input of the algorithm is an observed single-pointing spectrum, specified by its frequency and intensity. Our algorithm first queries a spectroscopic database in the observed frequency range and collects possible entries based on a user-defined list of molecules. Next, the algorithm sequentially performs fittings for all selected molecules, and then combines the fitting results using a greedy method. The combination process checks several criteria. Molecules that do not satisfy the criteria are put into a candidate list for manual review. Users can then decide whether to include a candidate. Ultimately, the

yishengq@zhejianglab.org

donghui.quan@zhejianglab.org

¹ <https://github.com/yqiuu/spectuner>

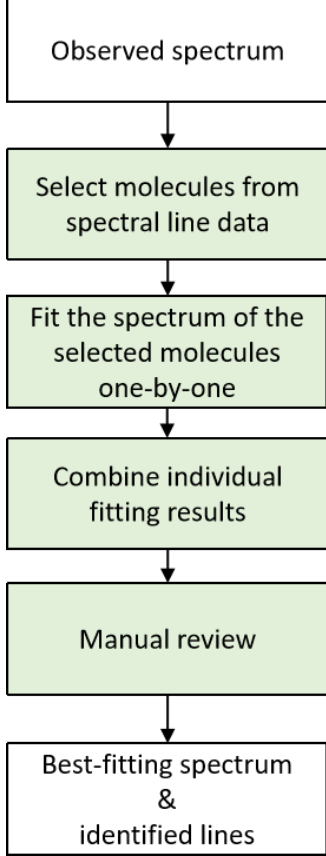


Figure 1. Flowchart of the proposed automated line identification framework. An overview of the algorithm is given in Section 2.1.

algorithm outputs the best-fitting spectrum and parameters, along with a table listing the identified lines.

We introduce the spectral line model and the spectroscopic database in Section 2.2. Our fitting techniques are detailed in Sections 2.3 and 2.4. The greedy method and the criteria for combining a fitting results are described in Section 2.5.

2.2. The spectral line model

This study employs XCLASS (Möller et al. 2017) to generate model spectra. The XCLASS code predicts model spectra by solving the one-dimensional radiative transfer equation for an isothermal object, assuming local thermodynamic equilibrium (LTE). In this study, we assume that the spectra of different molecules combine linearly, without considering any absorption features. The spectroscopic data are sourced from the Virtual Atomic and Molecular Data Center (VAMDC) (Endres et al. 2016), which contains entries from the Cologne Database for Molecular Spectroscopy (CDMS) (Müller et al. 2001, 2005) and the Jet Propulsion Laboratory (JPL) database (Pickett et al. 1998).

In this work, we fit the spectrum of a molecule, encompassing all possible states within the specified frequency range. Our code is capable of automatically selecting these possible states from the database.

In XCLASS, assuming a single component, the spectrum of one molecule of one state is characterized using five parameters: source size θ , excitation temperature T_{ex} , column density N_{tot} , velocity width Δv , and velocity offset v_{LSR} . We assume that source size, velocity width and velocity offset are shared among different states, while the other parameters are independent. This approach reduces the degrees of freedom, thereby simplifying the problem. All molecules considered in this work are assumed to consist of only one component for simplicity. In addition, we do not account for any absorption features in the spectrum. Frequency channels that are below the background temperature are set to this temperature.

2.3. Optimization

This study utilizes particle swarm optimization (PSO) (see e.g. Wang et al. 2018) for all fitting tasks. The algorithm, inspired by the social behavior of bird flocking, has a wide range of applications in both engineering and scientific fields. In the field of astronomy, PSO is applied to gravitational wave data analysis (Wang et al. 2014), calibration of semi-analytic galaxy formation models (Ruiz et al. 2015), and spectral energy distribution (SED) fitting (Qiu et al. 2023). Compared to the Levenberg–Marquardt algorithm, commonly used for spectral fitting, PSO offers several advantages. Firstly, PSO does not necessitate an initial guess from users. Instead, it selects initial points randomly within the specified parameter range. Secondly, the design of PSO balances exploration with exploitation, making it less prone to becoming trapped in local minima.

In practice, we apply the PSO proposed by Shi & Eberhart (1998). The initial positions are randomly drawn within the bounds specified in Table 1. The optimization algorithm executes for a minimum of N_{min} iterations, with

$$N_{\text{min}} = 100 + 5 \times (D - 5), \quad (1)$$

where D is the dimension of the problem. If the result fails to improve over 15 consecutive iterations, the optimization process will be halted. Moreover, a population size of 28 is adopted. This choice allows for running two tasks simultaneously on a single node of our high performance computing cluster. In general, a population size between 20 and 50 is preferred (Wang et al. 2018).

2.4. The peak matching loss function

Table 1. Summary of the bounds of the fitting parameters.

Name	Unit	Scale	Bounds
Source size θ	"	log	0.7 - 2.3
Excitation temperature T_{ex}	K	linear	10 - 400
Column density N_{tot}	cm^{-2}	log	12 - 20
Velocity width Δv	km/s	log	0.0 - 1.5
Velocity offset v_{LSR}	km/s	linear	-10 - 10

NOTE—Initial positions for optimization are randomly sampled within these bounds, and the optimizer ensures that the parameters do not exceed the bounds.

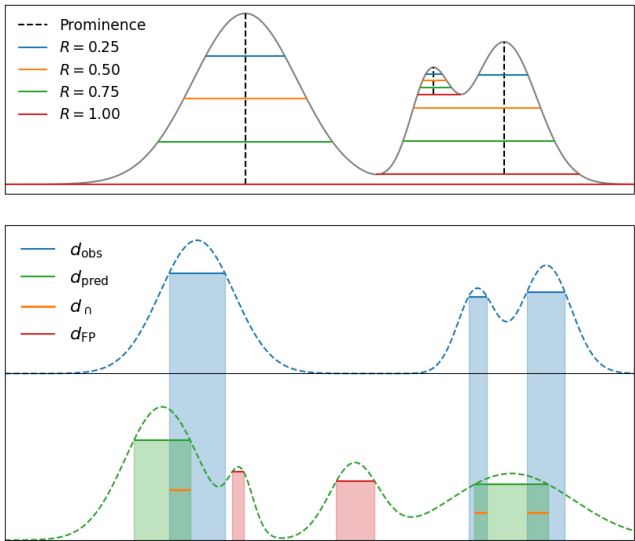


Figure 2. Schematics of some definitions in our peak finding algorithm as introduced in Section 2.4. In the upper panel, black dashed lines represent examples of prominence. Colored lines depict the peak widths estimated by the `peak_widths` function in SCIPY using various input parameters R , defined in Equation 4. The lower panel illustrates the interval intersection algorithm assuming that the blue dashed line is an observed spectrum and the green dashed line is a model spectrum. The definitions of d_{obs} , d_{pred} , d_{\cap} , and d_{FP} can also be found in the lower panel.

The loss function is a key component in optimization. Traditionally, the χ^2 loss has been widely used for spectral fitting. However, we find that applying χ^2 to perform fitting of a single molecule to observed spectra can be problematic and often leads to unsatisfactory results. The reason is that the χ^2 loss is sensitive to outliers, i.e. features that cannot be described by the model. Since observed spectra, especially line-rich spectra, consist of spectral lines from a variety of molecules, they include many features that the model spectrum of a single molecule cannot describe.

To address the above problem, this work proposes a peak matching loss function, which is able to robustly describe the distance between the observed and model spectra. Our idea is to only compare the spectra around the lines predicted by the spectral line model. The proposed loss function consists of three terms:

$$\mathcal{L}_{\text{PM}} = \mathcal{L}_{\text{MAE}} + \sum_{\text{TPPs}} \mathcal{L}_{\text{TP}} + \sum_{\text{FPPs}} \mathcal{L}_{\text{FP}}. \quad (2)$$

The first term is known as the mean absolute error (MAE), which is less sensitive to outliers and is commonly used in machine learning context. It is defined as

$$\mathcal{L}_{\text{MAE}} = \frac{1}{N} \sum_{i=0}^N \left| T_i^{\text{obs}} - T_i^{\text{pred}} \right|, \quad (3)$$

where N is the number of observed frequency channels.

To calculate the second and third terms, a peak finding algorithm must be applied to both observed and model spectra. This work adopts the `find_peaks` and `peak_widths` functions implemented in SCIPY (Virtanen et al. 2020) to identify peaks. The algorithm includes a parameter, namely the required prominence, which is essential for our application. Prominence is a property of a peak, defined as the vertical distance from the peak height to the lowest contour line that does not enclose any higher peak. Examples of prominence are given in the upper panel of Figure 2. The peak finder only identifies peaks with a prominence greater than the specified prominence threshold. In this study, the prominence threshold is set at four times the root mean square (RMS) noise. Additionally, our peak finder is designed to ignore peaks based on a predefined list of central frequencies. This function is useful for ignoring known radio recombination lines.

After calling `find_peaks`, we use `peak_widths` to estimate the width of each peak. The widths are evaluated at h_{width} defined as

$$h_{\text{width}} = h_{\text{peak}} - P \times R, \quad (4)$$

where h_{peak} is the peak height, P is the prominence of the peak, and R is a user-defined parameter. The choice of R is subtle. As illustrated in the lower panel in Figure 2, too large values of R could result in the blending of several peaks, while too small values of R might cause instability in calculating our peak matching loss function. Based on our experience, setting $R = 0.25$ is a practical choice.

The objective of the aforementioned step is to characterize the peaks within a spectrum through an array of intervals defined by their central frequency and width. Once we obtain the intervals of both observed and model

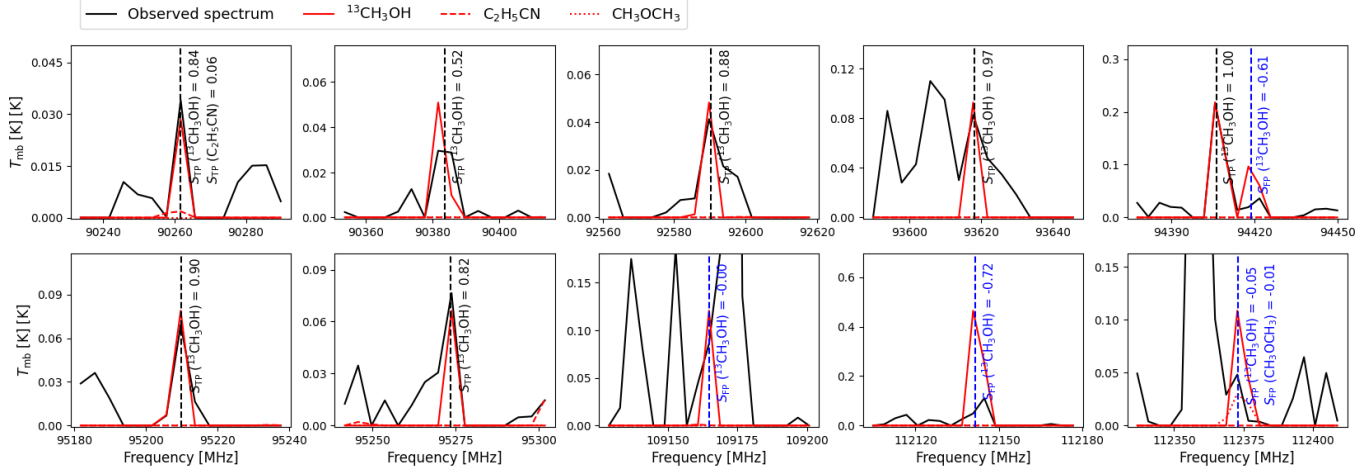


Figure 3. Visualization of S_{TP}^i and S_{FP}^i defined in Equations 18 to 22. Black solid lines illustrate the observed spectrum of *W51-Mopra* (see Section 3.1). Red lines show the best-fitting spectra of $^{13}\text{CH}_3\text{OH}$, $\text{C}_2\text{H}_5\text{CN}$ and CH_3OCH_3 obtained with the peak matching loss in the combined phase. The complete identification results for *W51-Mopra* are presented in Section 4. Each black (blue) vertical line represents a true (false) positive peak identified using our peak finding algorithm as described in Section 2.4.

spectra, we apply an interval intersection algorithm to classify the peaks of the model spectrum as true and false positive peak. If an interval from the model spectrum intersects with an interval of the observed spectrum, the associated peak is labeled as a true positive peak (TPP), while if the condition is not satisfied, the corresponding peak is classified as a false positive peak (FPP). Illustrations of true and false positive peaks are presented in the lower panel of Figure 2.

The second term in Equation 2 rewards true positive peaks (TPPs), which is defined as

$$\mathcal{L}_{\text{TP}} = \begin{cases} D_{\text{TP}} - f_{\text{dice}} I^{\text{obs}}, & I^{\text{obs}} \geq I^{\text{pred}}, \\ \min(D_{\text{TP}} - f_{\text{dice}} I^{\text{obs}}, 0), & I^{\text{obs}} < I^{\text{pred}}, \end{cases} \quad (5)$$

with

$$f_{\text{dice}} = \frac{2d_{\cap}}{d_{\text{obs}} + d_{\text{pred}}}, \quad (6)$$

$$D_{\text{TP}} = \frac{1}{d_{\cap}} \int_{d_{\cap}} |T_{\nu}^{\text{obs}} - T_{\nu}^{\text{pred}}| d\nu, \quad (7)$$

$$I_{\text{obs}} = \frac{1}{d_{\text{obs}}} \int_{d_{\text{obs}}} |T_{\nu}^{\text{obs}} - T^{\text{back}}| d\nu, \quad (8)$$

$$I_{\text{pred}} = \frac{1}{d_{\text{pred}}} \int_{d_{\text{pred}}} |T_{\nu}^{\text{pred}} - T^{\text{back}}| d\nu, \quad (9)$$

where d_{\cap} , d_{obs} , and d_{pred} are shown in the lower panel of Figure 2. The use of f_{dice} has two effects. First, it smooths the transition between the cases with and without intersection. Secondly, it could measure the similarity in shape between two peaks. When computing the integrals in Equations 7, 8, and 9, the trapezoidal rule is adopted. Within the interval, we only use channels

given by the observed spectrum, without including any additional points, while linear interpolation is applied at the boundaries. Equation 2 can yield negative values when true positive peaks (TPPs) are identified, signifying a strong correspondence between the peaks in the observed and model spectra.

The third term in Equation 2 penalizes false positive peaks (FPPs). Its definition is given by

$$\mathcal{L}_{\text{FP}} = D_{\text{FP}} W(\nu_{\text{FP}}), \quad (10)$$

with

$$D_{\text{FP}} = \min(D_1, D_2) \quad (11)$$

$$D_1 = \frac{1}{d_{\text{FP}}} \int_{\text{FP}} \max(T_{\nu}^{\text{pred}} - T_{\nu}^{\text{obs}}, 0) d\nu \quad (12)$$

$$D_2 = \frac{1}{d_{\text{FP}}} \int_{\text{FP}} \max(T_{\nu}^{\text{pred}} - T^{\text{back}} - P, 0) d\nu \quad (13)$$

$$W(\nu) = \begin{cases} \frac{\nu - \nu_{\text{left}}}{\nu_{\text{mid}} - \nu_{\text{left}}}, & \nu < \nu_{\text{mid}}, \\ \frac{\nu_{\text{right}} - \nu}{\nu_{\text{right}} - \nu_{\text{mid}}}, & \nu \geq \nu_{\text{mid}}, \end{cases} \quad (14)$$

$$\nu_{\text{mid}} = \frac{1}{2}(\nu_{\text{left}} + \nu_{\text{right}}), \quad (15)$$

where P is the value of the prominence and ν_{FP} is the central frequency of the false positive peak. ν_{left} and ν_{right} are the central frequencies of the nearest observed peaks on the left and right sides respectively. The trapezoidal rule is adopted to compute Equations 12 and 13. If a false positive peak is hidden in a broad observed peak, e.g. the left false positive peak in the lower panel of Figure 2, there is no need to penalize it, and therefore we introduce a maximum operation in Equations 12 and 13. The use of D_2 is to smooth the transition between

the cases if a local maximum is identified and not identified as a peak. $W(\nu)$ allows to reduce \mathcal{L}_{FP} by shifting the central frequency in addition to decreasing T_{ν}^{pred} .

2.5. Combining individual fitting results

This work proposes a greedy algorithm to combine individual fitting results (see Algorithm 1). In the algorithm, a "pack" consists of a molecule list, model parameters and model spectrum, which can initiate a new fitting. The algorithm input is a list of packs, each constructed from individual fitting results. The algorithm outputs a combined result and fitting results of some candidate molecules which do not satisfy the criteria described in the following paragraph.

The proposed algorithm adopts two scores to decide whether an individual fitting result can be incorporated. First, the total score is defined as

$$S_{\text{tot}}^i = \sum_{\text{TPPs}} S_{\text{TP}}^i + \sum_{\text{FPPs}} S_{\text{FP}}^i, \quad (16)$$

with

$$S_{\text{tot}}^i = \sum_{\text{TPPs}} S_{\text{TP}}^i + \sum_{\text{FPPs}} S_{\text{FP}}^i, \quad (17)$$

$$S_{\text{TP}}^i = F_{\text{TP}}^i \max \left(1 - \frac{D_{\text{TP}}^i}{I_{\cap}^i}, 0 \right), \quad (18)$$

$$F_{\text{TP}}^i = \frac{I_{\cap}^i}{\sum' I_{\cap}^i}, \quad (19)$$

$$I_{\cap}^i = \frac{1}{d_{\cap}} \int_{d_{\cap}} |T_{\nu}^{\text{pred},i} - T^{\text{back}}| d\nu, \quad (20)$$

$$S_{\text{FP}}^i = -F_{\text{FP}}^i \frac{D_{\text{FP}}^i}{I_{\text{pred}}^i}, \quad (21)$$

$$F_{\text{FP}}^i = \frac{I_{\text{pred}}^i}{\sum_i I_{\text{pred}}^i}, \quad (22)$$

where I_{pred}^i , D_{TP}^i , and D_{FP}^i are defined in Equations 9, 7, and 11. These quantities here are computed for each molecule. We note that a true (or false) positive peak can be contributed by multiple molecules, and we use F_{TP}^i and F_{FP}^i to take into account the different contributions. In the calculation of F_{TP}^i and F_{FP}^i , contributions less than 5% are excluded beforehand, resulting in renormalized fractions. Figure 3 provides a visualization of S_{TP}^i and S_{FP}^i .

We further define S_X^i as the X -th largest value among S_{TP}^i of all true positive peaks. If the number of true positive peaks is smaller than X , S_X^i is set to zero.

Our criteria to combine a fitting result are

$$S_3^i > 0.8 \text{ and } S_{\text{tot}}^i > 2.7. \quad (23)$$

Satisfying these criteria implies that at least three lines are matched. Specifically, the lower limit of S_3^i ensures that the model spectrum has at least three matched lines with a score exceeding 0.8, while S_{tot}^i imposes additional constraints on the average score and accounts for false positive peaks. We note that these values are purely empirical but lead to reasonable results. Users have the flexibility to adjust the criteria according to their specific applications.

We point out that a more straightforward method for combining all individual fitting results could involve simultaneously fitting the spectrum of all molecules. However, this method is considered to be impractical. The large number of molecules involved in the fitting task results in an excessive number of free parameters (~ 100 to 500), which requires considerable iterations for the optimizer to attain convergence. In contrast, our greedy algorithm is more efficient. Furthermore, due to the intricacy of the spectral lines, there are various choices for combining the individual fitting results, and our algorithm offers an interpretable solution.

3. DATA

In this work, we assess our algorithm for automated line identification using data from five published line surveys.

3.1. W51-Mopra

We utilize the published data from [Watanabe et al. \(2017\)](#), who conducted a line survey towards the W51 region using the Mopra 22 m telescope. The survey covers the frequency ranges from 85.2 - 101.1 GHz and 107.0 - 114.9 GHz. The spectral data originate from the hot cores e1/e2, located at galactic coordinate $(l, b) = (49^{\circ}.4898, -0^{\circ}.3874)$. [Watanabe et al. \(2017\)](#) identified 234 emission lines. The faintest line has a peak temperature of 60 mK, detected at $\sim 4.5\sigma$ level.

We adopt the RMS noise values of 20 mK and 70 mK for 85.2 - 101.1 GHz and 107.0 - 114.9 GHz respectively, as indicated in Figure 2 of [Watanabe et al. \(2017\)](#). These values serve as inputs for our peak finding algorithm. In addition, their table of identified lines includes six radio recombination lines, which are excluded by our peak finder.

3.2. OrionKL-GBT

This study relies on the data published by [Frayer et al. \(2015\)](#), who conducted a line survey towards Orion KL. The observations were carried out using the Green Bank Telescope (GBT) and were centered on the celestial coordinates R.A. (J2000) 05:35:14, decl. (J2000) 05:22:27.5. The frequency range covered by the survey

Algorithm 1: Combining individual fitting results

```

# The algorithm is introduced in Section 2.5, including the criteria to accept a result.
Input: pack_list
Output: pack_combined, cand_list
Sort pack_list by loss in ascending order;
Set cand_list as an empty list;
pack_combined  $\leftarrow$  None;
# Determine the first pack that can be merged.
i_pack  $\leftarrow$  0;
for i = 0, ..., len(pack_list) do
    pack  $\leftarrow$  pack_list[i];
    Estimate the scores for pack;
    if the scores satisfy the criteria then
        | pack_combined  $\leftarrow$  pack;
        | break;
    else
        | Put pack into cand_list;
    end
    i_pack  $\leftarrow$  i_pack + 1;
end

# Merge the remaining packs.
for i = i_pack + 1, ..., len(pack_list) do
    pack  $\leftarrow$  pack_list[i];
    if pack has overlapped lines with pack_combined then
        | Use pack to start a new fitting, including the best-fitting parameters of pack in the initialization of the optimizer
        | and setting the spectrum of pack_combined as background;
        | Overwrite pack using the new fitting result;
    end
    Combine pack_combined with pack to estimate the scores for pack;
    if the scores satisfy the criteria then
        | Merge pack into pack_combined;
    else
        | Put pack into cand_list;
    end
end

# Perform a new fitting for all candidates.
for i = 0, ..., len(cand_list) do
    pack  $\leftarrow$  cand_list[i];
    if pack has overlapped lines with pack_combined then
        | Use pack to start a new fitting and set the spectrum of pack_combined as background;
        | Overwrite pack using the new fitting result;
        | cand_list[i]  $\leftarrow$  pack;
    end
end

```

spans from 67.0 GHz to 93.6 GHz. Frayer et al. (2015) only identified lines with intensities brighter than 1 K, and in total, 140 emission lines were identified.

As input for our peak finder, we adopt three RMS noise levels: 66.5 mK for 67.0 GHz to 70.0 GHz, 31.6 mK for 70.0 GHz to 85 GHz, and 41.2 mK for 85.0 GHz to 93.6 GHz. These values are estimated from their Table 1. Frayer et al. (2015) identified three lines from atmospheric O₂, which are ignored by our peak finder.

3.3. OrionKL-Tianma

We incorporate the data from Liu et al. (2022), who carried out a line survey targeting the Orion KL region using the Tianma 65 m radio telescope. The spectral data are centered on the celestial coordinates R.A. (J2000) 05:35:14.55, decl. (J2000) -05:22:31.0. The frequency coverage spans from 34.5 GHz to 50.0 GHz. A total of 597 emission lines were identified, including 177 classified as radio recombination lines. The faintest line detected has a peak intensity of 2.8 mK.

For the peak finder, we adopt two RMS noise values, at 4 mK and 7 mK for 34.5 GHz - 48.7 GHz and 48.7

GHz - 50.0 GHz respectively. We estimate these values from Figure 3 in [Liu et al. \(2022\)](#). All radio recombination lines identified by [Liu et al. \(2022\)](#) are ignored by our peak finder.

3.4. *SgrB2M-IRAM and SgrB2N-IRAM*

The most complex test data utilized in this study originate from [Belloche et al. \(2013\)](#), who presented a line identification analysis for both Sgr B2(M) and B2(N) within the frequency range of 80.0 GHz to 116.0 GHz. The observations were conducted using the IRAM 30 m telescope, targeting the positions at R.A. (J2000) 17:47:20s.4, decl. (J2000) -28:23:07.0 for Sgr B2(M), and R.A. (J2000) 17:47:20.0 and decl. (J2000) -28:22:19.0 for and B2(N), respectively. These sources are line rich. [Belloche et al. \(2013\)](#) identified 945 and 3675 emission lines in Sgr B2(M) and B2(N) respectively.

In terms of the RMS noise required by our peak finder, we use four values as listed in Table 1 in [Belloche et al. \(2013\)](#).

4. APPLYING TO LINE SURVEYS

In this study, for speed reason, we downsample all observed spectra by averaging every two adjacent channels. The downsampling is repeated three times. Accordingly, the number of channels in the observed spectra is reduced by a factor of eight, and the RMS noise values are divided by $\sqrt{8}$ before being input into the peak finding algorithm. Secondly, for simplicity, this work neglects any absorption in the observed spectra. Given that the baselines of all the observed spectra used in this work have been calibrated to zero by the original studies, our correction is straightforward. Specifically, any channels displaying a negative value are reset to zero. In addition, the continuum spectra are not taken into account in the fitting processes.

In addition, our algorithm requires a molecule list as input. Since this work focuses on whether our method can reproduce the identification results of the previous studies rather than identifying new molecules, we use the molecules identified in previous studies as input. For practical use, our code provides a list of commonly observed molecules, e.g. methanol (CH_3OH), methyl formate (CH_3OCHO) and cyanoacetylene (HCCCN). Users can customize the molecule list to suit their specific applications.

4.1. *Metrics*

In this work, we use recall to compare our identification results with the published line survey data. The recall of this work is computed as follows. The denominator is the number of relevant lines, i.e. lines both in

the line table of the test data and identified by our peak finding algorithm. When counting the relevant lines, the following points are taken into account:

1. If a frequency is labeled by multiple species, the corresponding lines are excluded.
2. A peak can be comprised of multiple spectral lines from the same molecule. In this case, the lines are merged into one.
3. The line surveys may use different spectral line databases, and to be consistent, we only include lines that exist in the spectral line database used in this work.
4. Radio recombination lines are excluded.

The numerator of the recall is the number of lines labeled by our identification algorithm that matches the test data.

4.2. *Results*

[Table 2](#) shows the overall recall obtained from the test data. The overall recalls achieved using the peak matching loss are 84% - 98%, consistently higher than using the χ^2 loss.

We illustrate the issue with using the χ^2 loss function through an example. In [Figure 4](#), we present the fitting results of $\text{C}_2\text{H}_3\text{CN}$ during the individual fitting phase for *SgrB2N-IRAM*. The results based on the peak matching and χ^2 loss functions are represented by red and blue lines respectively. It is evident that the red line gives a better result than the blue line. However, upon calculating the χ^2 and peak matching loss values for both fits, we find that the χ^2 value of the blue line ($\chi^2 = 12780.4$) is smaller than the red line ($\chi^2 = 12780.9$). In other words, if the χ^2 loss is adopted, the algorithm will consider the blue line as a better result than the red line, irrespective of optimization methods. Such result is unexpected. In contrast, the proposed peak matching loss assigns a lower value to the red line ($\mathcal{L}_{\text{PM}} = -2.79$) than the blue line ($\mathcal{L}_{\text{PM}} = 1.40$), which appropriately reflects the variance between the observed and fitting spectra.

4.2.1. *W51-Mopra*

We illustrate the best-fitting spectrum for *W51-Mopra* in [Figure 5](#), and show the recalls in [Figure 6](#). When adopting the peak matching loss function, our algorithm attains an overall recall of 91%, 13% better than using the χ^2 loss function. The recall of methanol stands relatively low, at 62%. Our analysis suggests that the spectrum of methanol can be better described by more

Table 2. Summary of the line survey data used in this study and the recalls attained using our automated line identification algorithm.

Name	Frequency coverage (GHz)	Line density (GHz ⁻¹)	Recall (χ^2)	Recall (PM)	Duration (PM) (hour)
<i>W51-Mopra</i>	85.2 - 101.1, 107.0 - 114.9	13.8	78% (118/152)	91% (139/152)	8.6
<i>OrionKL-GBT</i>	67.0 - 93.6	20.3	86% (90/105)	98% (103/105)	5.6
<i>OrionKL-Tianma</i>	34.5 - 50.0	30.5	59% (140/237)	87% (207/237)	14.8
<i>SgrB2M-IRAM</i>	80.0 - 116.0	38.0	60% (276/463)	85% (392/463)	25.6
<i>SgrB2N-IRAM</i>	80.0 - 116.0	59.2	47% (498/1055)	84% (881/1055)	59.0

NOTE—The total number of lines for estimating line density is obtained using our peak finder described in Section 2.4. Recall, defined in Section 4.1, is a metric to evaluate our algorithm. The last column indicates the duration of the automated line identification process with the peak matching loss function. All tasks are conducted using 28 2.6 GHz CPUs in parallel.

than one component. As demonstrated in Figure 7, by adding an additional component, the best-fitting spectrum of methanol is improved, and the recall increases to 96%.

4.2.2. *OrionKL-GBT*

For *OrionKL-GBT*, the best-fitting spectrum and the recalls of the molecules are demonstrated in Figure 8 and 9 respectively. Frayer et al. (2015) only identified lines that are brighter than 1 K, which is significantly higher than the RMS noise. Therefore, we obtain the best results on *OrionKL-GBT*, achieving a recall of 98 %. Our algorithm fails to identify one line for thioformaldehyde (H₂CS). The reason is that our method identified three alternative lines as illustrated in Figure 10.

4.2.3. *OrionKL-Tianma*

In terms of *OrionKL-Tianma*, we demonstrate the best-fitting spectra and the recalls in Figure 11 and Figure 12 respectively. The best-fitting spectrum using χ^2 shows considerable wrong features, and a potential reason is that the observed spectrum consists of over 100 strong radio recombination lines, which disturbs the fitting. In contrast, the result using the peak matching loss function well agrees with the observed spectrum, indicating the robustness of our method.

The result using the peak matching loss function only identifies about half acetone (CH₃COCH₃) lines, missing 9 lines. In fact, our method reproduces the right features, while these features are slightly below the threshold of our peak finding algorithm. Consequently, these features are not counted in computing the recall. We demonstrate this point in Figure 13. The similar problem is also found in the results of CH₃OCHO, C₂H₅CN, and ³⁴SO₂.

In addition, as discussed by Liu et al. (2022), the detected SiO emission is complex and involves masers, which cannot be described using only one velocity com-

ponent. Therefore, our algorithm fails to identify all the SiO lines.

Figure 14 compares the parameters estimated by Liu et al. (2022) with our best-fitting parameters. Whenever the original study suggested multiple components, the component with the highest column density is compared. For each molecule, Liu et al. (2022) used fixed values for the source size and excitation temperature, and fit the column density, velocity width, and velocity offset. In Figure 14, for the result based on the peak matching loss, we find that the column density and velocity offset are generally consistent, whereas the source size, excitation temperature, and velocity width are inconsistent. The result using the χ^2 loss tends to predict larger velocity widths.

4.2.4. *SgrB2M-IRAM*

We show the best-fitting spectra for *SgrB2M-IRAM* in Figure 15, and the recalls are given in Figure 16. While the result using the χ^2 loss function achieves an overall recall of 60%, the best fitting spectrum is fundamentally flawed. In contrast, in such line rich region, our result using the peak matching loss fits the observed spectrum well, with an overall recall of 85 %.

The result using the peak matching shows a low recall of ethanol (C₂H₅OH), which is mainly due to line blending. To illustrate the point, we show the best fitting spectrum of C₂H₅OH in the individual fitting phase as blue lines, which can match most of the lines. However, by comparing the result obtained in the individual fitting phase with the final spectrum, we can find line blending at 82650.97 MHz, 102487.53 MHz, 106648.67 MHz, and 114066.018 MHz.

Our results also attain low recalls of HCCCN and CH₃OH. These molecules tend to be better described by multiple physical components, while our method assumes one component for each molecule for simplicity. This issue is also mentioned in Section 4.2.1.

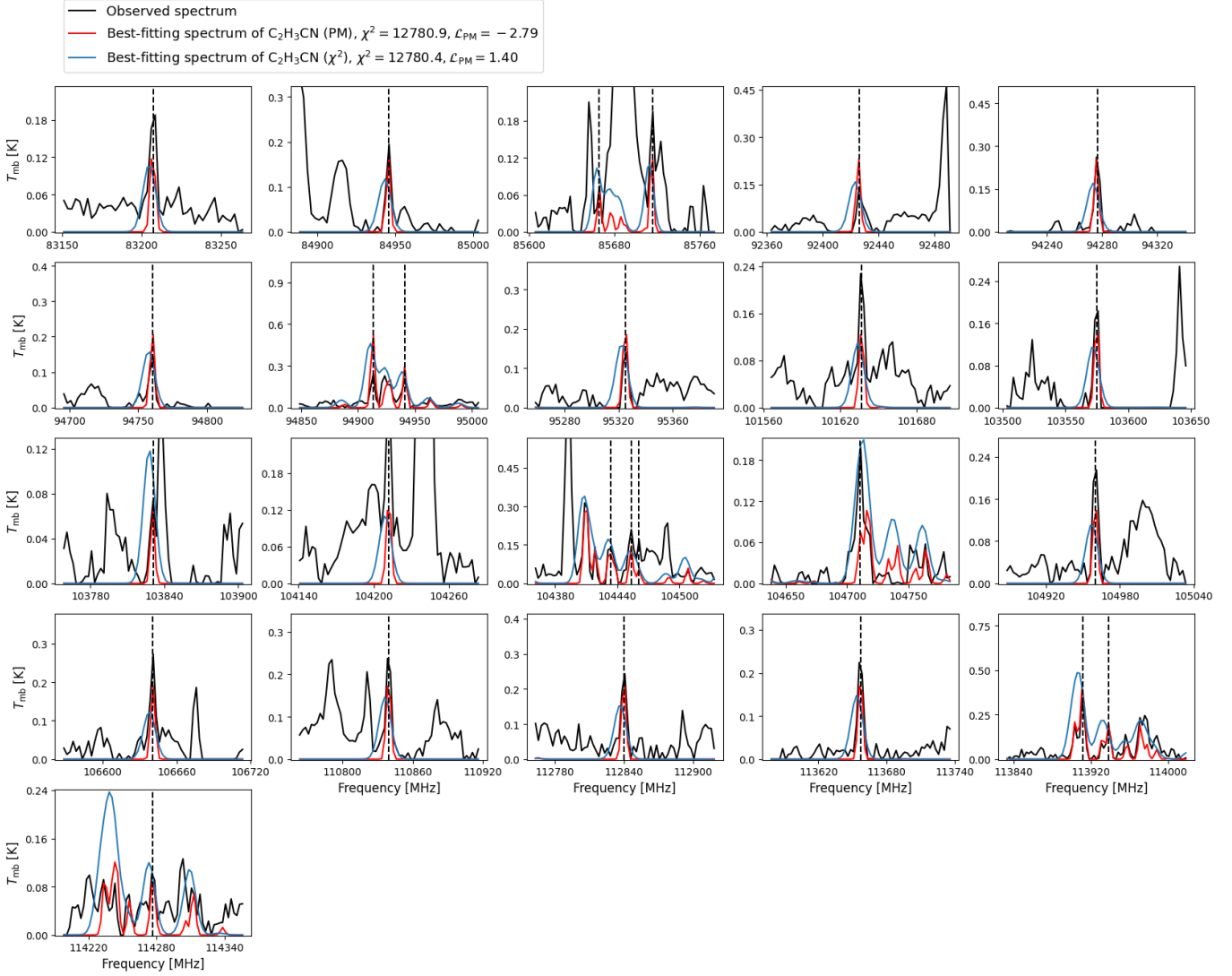


Figure 4. Comparison of the best-fitting spectra using different loss functions. Black solid line illustrates the observed spectrum of *SgrB2M-IRAM* (see Section 3.4), and blue dashed lines represent the spectral lines of C₂H₃CN identified by Belloche et al. (2013). Blue and red lines demonstrate the best-fitting results achieved with the χ^2 and peak matching loss functions respectively. The peak matching loss function is defined in Section 2.4. We compute and display both the χ^2 and peak matching loss values corresponding to each best-fitting spectrum. These values imply that using the χ^2 loss is inappropriate for spectral fitting of a single molecule.

In Figure 18, we compare the estimated parameters from Belloche et al. (2013) with our results. Whenever the original study suggests multiple components, the component with the highest column density is compared. Belloche et al. (2013) also generated the spectrum using XCLASS. While a correlation is found for the column density, our results based on the peak matching loss tend to underestimate it by 1 - 2 dex. A potential reason could be that our algorithm tends to adopt larger source sizes than Belloche et al. (2013). Moreover, no significant correlation can be found for the other parameters.

4.2.5. *SgrB2N-IRAM*

For *SgrB2N-IRAM*, we show the best-fitting spectra and the recalls in Figures 19 and 20 respectively. *SgrB2N-IRAM* is the most challenging test data in this study, with a line density of 59.2 GHz⁻¹. In this case, we only attain an overall recall of 37% when using the χ^2 loss, and the best-fitting spectrum is not meaningful. In contrast, the result based on the peak matching loss still reaches an overall recall of 84%, and the best-fitting spectrum is in good agreement with the observation.

Our results attain low recalls of CH₃¹³CH₂CN and CH₂(OH)CHO. We attribute this to line blending, similar to the case of C₂H₅OH in *SgrB2M-IRAM*.

The identification of cyclopropenylidene ($c\text{-C}_3\text{H}_2$) is special, which is affected by absorption in the observed spectrum. Figure 21 illustrates the spectrum of $c\text{-C}_3\text{H}_2$ generated using the parameters suggested by Belloche et al. (2013). Absorption features are found at the locations of three peaks, at 82093.63MHz, 85339.04MHz, and 87435.74 MHz. If the absorption component is modeled properly, these three peaks will be attenuated. However, this work does not model absorption, and the absorbed spectrum is simply set to zero. Consequently, the three peaks are treated as false positive peaks in our algorithm, resulting in a higher loss. Whereas our result identifies the spectral lines of $c\text{-C}_3\text{H}_2$, our algorithm cannot handle the case associated with absorption in general.

In addition, our algorithm fails to identify HNCS, CH_3COOH , and HNC^{18}O . We find it difficult to reproduce the spectral lines of these molecules using the parameters suggested by Belloche et al. (2013). A potential reason could be that different spectral data were used.

In Figure 22, we compare the parameters suggested by Belloche et al. (2013) with our best-fitting parameters. Both results employ XCLASS to generate model spectra. Similar to *SrgB2M-IRAM*, we can only find correlation for the column density, and the other parameters show discrepancies.

4.3. Computational cost

For all line surveys considered in this study, the automated line identification algorithm is executed using 28 2.6 GHz CPUs in parallel. When employing the peak matching loss function, the time spent on each line survey is given in Table 2. The computational cost varies from 5.6 to 59.0 hours, depending on the complexity of the observed spectrum.

5. SUMMARY

To summarize, we develop a framework for automated line identification of interstellar molecules. Our main contributions are summarized as follows.

- We propose the peak matching loss function, which significantly enhances the robustness of spectral fitting. Our results using the peak matching loss are consistently better than using the widely used χ^2 loss. It is worth noting that the peak matching loss function is an independent component in our method, and in principle can be incorporated into other codes to improve the fitting results.

- We develop a greedy algorithm to combine the fitting results of individual molecules. The algorithm is efficient and interpretable.

We evaluate our algorithm using published data of five line surveys, including line rich regions in Sgr B2. Our algorithm achieves an overall recall of 84% - 98%. The errors of our algorithm are mainly due to the following factors:

- Due to the stochastic nature of particle swarm optimization, our results involve random errors.
- While our method assumes a single physical component for all molecules for simplicity, certain molecules, e.g. methanol, might be better described by incorporating multiple components.
- Line blending can result in ambiguity and multiple possible solutions.
- Absorption in the spectrum can affect spectral fitting.

We also compare our best-fitting parameters with the previous studies. Whereas our best-fitting spectra are in good agreement with the observations, the estimated parameters are in general inconsistent with the previous studies. We find a correlation only for the column density, with an error of two orders of magnitude. We attribute this discrepancy to the inherent degeneracy between the source size, excitation temperature, and column density.

Our method contributes to significantly reducing the workload of spectral line identifications. The results produced by our method provide an excellent starting point for a more detailed analysis.

¹ This work was supported by the National Natural Science Foundation of China under grant 12373026, and the Leading Innovation and Entrepreneurship Team of Zhejiang Province of China (Grant No. 2023R01008).
² The computation is performed at the Shuguang supercomputer in Zhejiang Laboratory.

Facilities: GBT 100 m, IRAM 30 m, Mopra 22 m, Tianma 65 m (TMRT).

Software: MATPLOTLIB (Hunter 2007), NUMPY (Harris et al. 2020), PANDAS (Wes McKinney 2010; pandas development team 2020), SCIPY (Virtanen et al. 2020), XCLASS (Möller et al. 2017).

REFERENCES

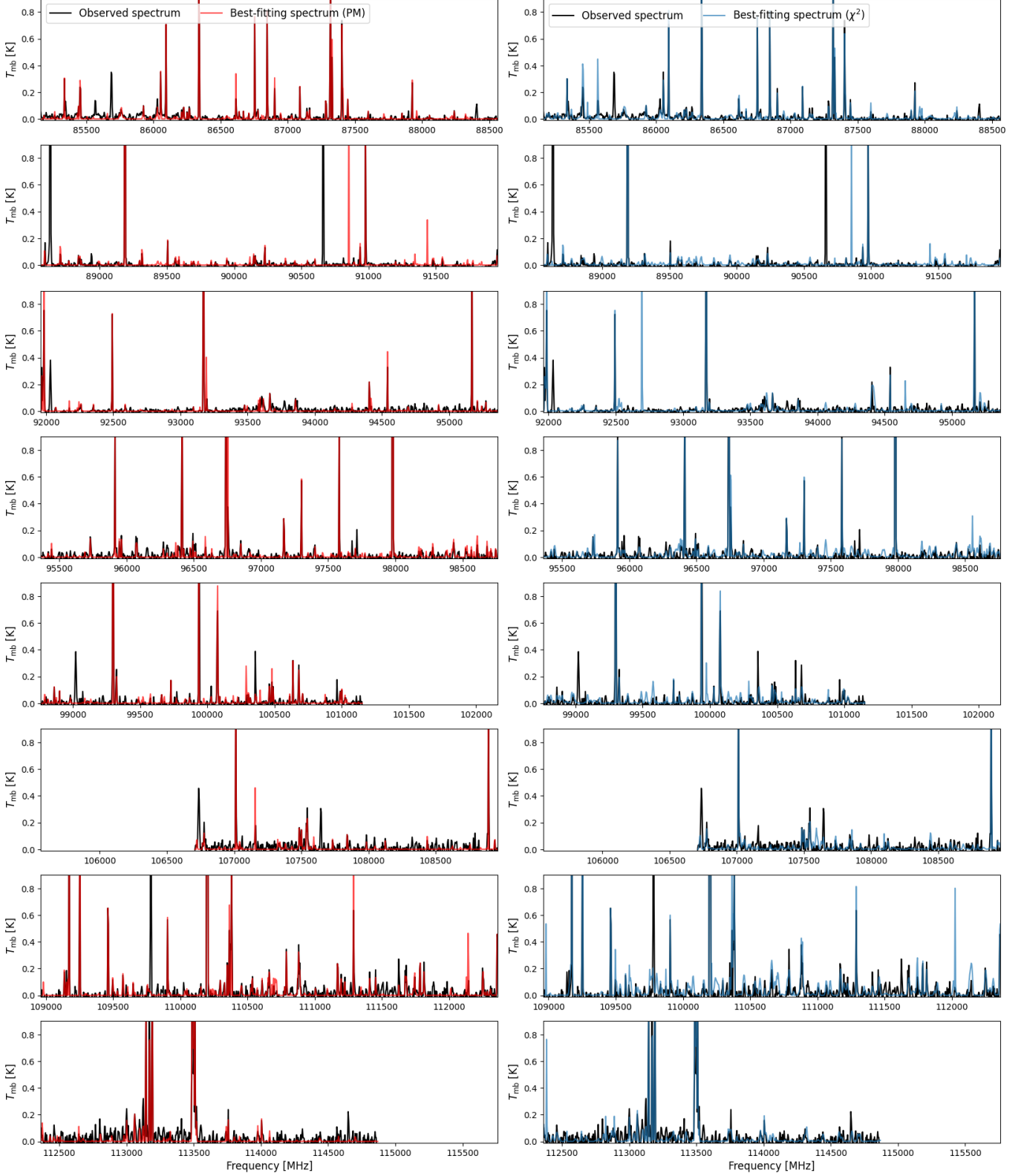


Figure 5. Best fitting results for *W51-Mopra*. Black lines represent the observed spectrum. Left and right panels show the results using the peak matching and χ^2 loss functions respectively. The peak matching loss function is described in Section 2.4.

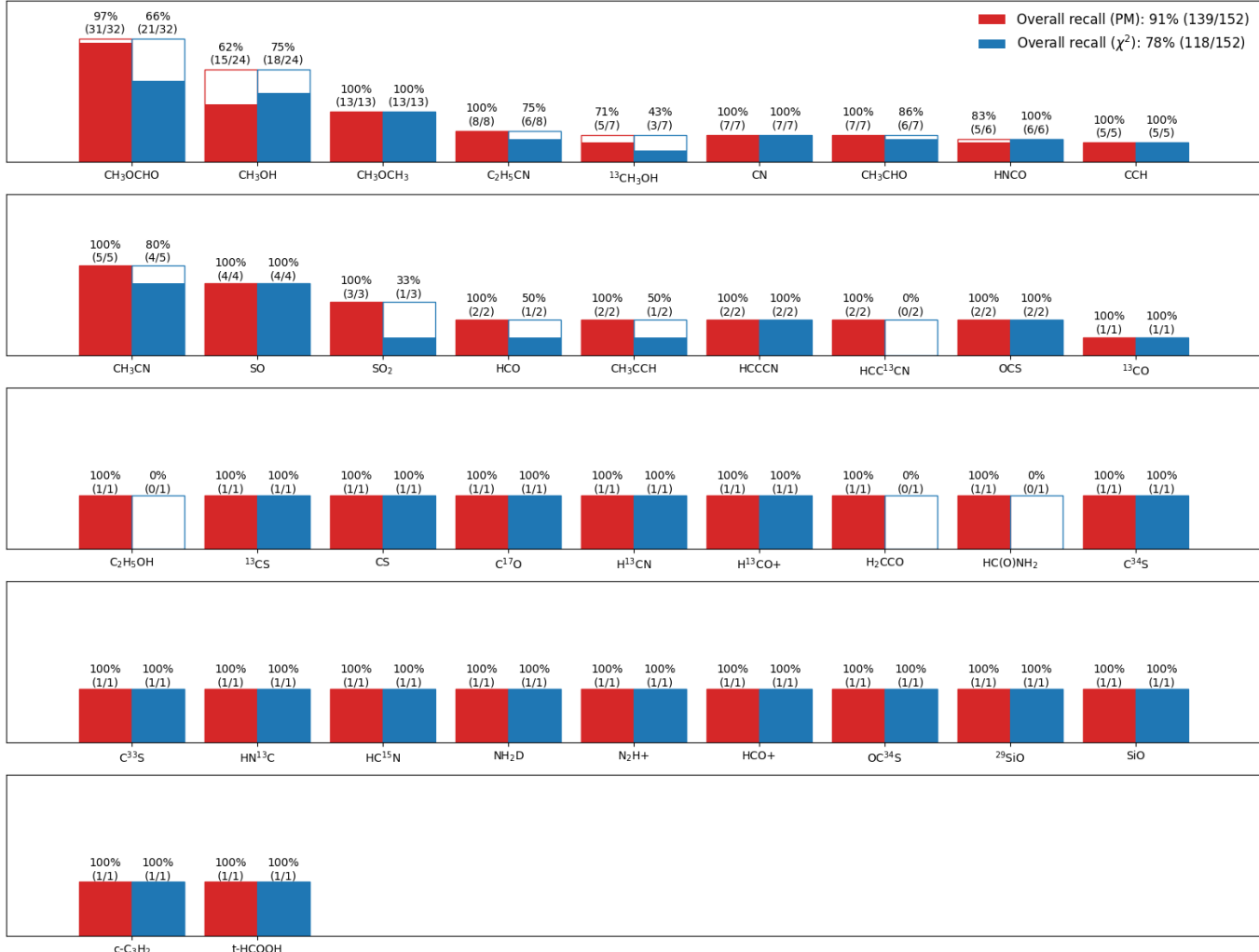


Figure 6. Recall of molecules identified in *W51-Mopra*. Red and blue bars illustrate the results using the peak matching and χ^2 loss functions respectively. The recall, the number of matched lines, and the number of relevant lines are indicated on top of each bar. Refer to Section 4.1 for the definition of recall.

Belloche, A., Müller, H. S. P., Menten, K. M., Schilke, P., & Comito, C. 2013, A&A, 559, A47, doi: [10.1051/0004-6361/201321096](https://doi.org/10.1051/0004-6361/201321096)

Endres, C. P., Schlemmer, S., Schilke, P., Stutzki, J., & Müller, H. S. P. 2016, Journal of Molecular Spectroscopy, 327, 95, doi: [10.1016/j.jms.2016.03.005](https://doi.org/10.1016/j.jms.2016.03.005)

Frayer, D. T., Maddalena, R. J., Meijer, M., et al. 2015, AJ, 149, 162, doi: [10.1088/0004-6256/149/5/162](https://doi.org/10.1088/0004-6256/149/5/162)

Ginsburg, A., Sokolov, V., de Val-Borro, M., et al. 2022, AJ, 163, 291, doi: [10.3847/1538-3881/ac695a](https://doi.org/10.3847/1538-3881/ac695a)

Harris, C. R., Millman, K. J., van der Walt, S. J., et al. 2020, Nature, 585, 357, doi: [10.1038/s41586-020-2649-2](https://doi.org/10.1038/s41586-020-2649-2)

Hunter, J. D. 2007, Computing in Science & Engineering, 9, 90, doi: [10.1109/MCSE.2007.55](https://doi.org/10.1109/MCSE.2007.55)

Liu, X., Liu, T., Shen, Z., et al. 2022, ApJS, 263, 13,

doi: [10.3847/1538-4365/ac9127](https://doi.org/10.3847/1538-4365/ac9127)

Maret, S., Hily-Blant, P., Pety, J., Bardeau, S., & Reynier, E. 2011, A&A, 526, A47, doi: [10.1051/0004-6361/201015487](https://doi.org/10.1051/0004-6361/201015487)

Martín, S., Martín-Pintado, J., Blanco-Sánchez, C., et al. 2019, A&A, 631, A159, doi: [10.1051/0004-6361/201936144](https://doi.org/10.1051/0004-6361/201936144)

Möller, T., Endres, C., & Schilke, P. 2017, A&A, 598, A7, doi: [10.1051/0004-6361/201527203](https://doi.org/10.1051/0004-6361/201527203)

Müller, H. S. P., Schlöder, F., Stutzki, J., & Winnewisser, G. 2005, Journal of Molecular Structure, 742, 215, doi: [10.1016/j.molstruc.2005.01.027](https://doi.org/10.1016/j.molstruc.2005.01.027)

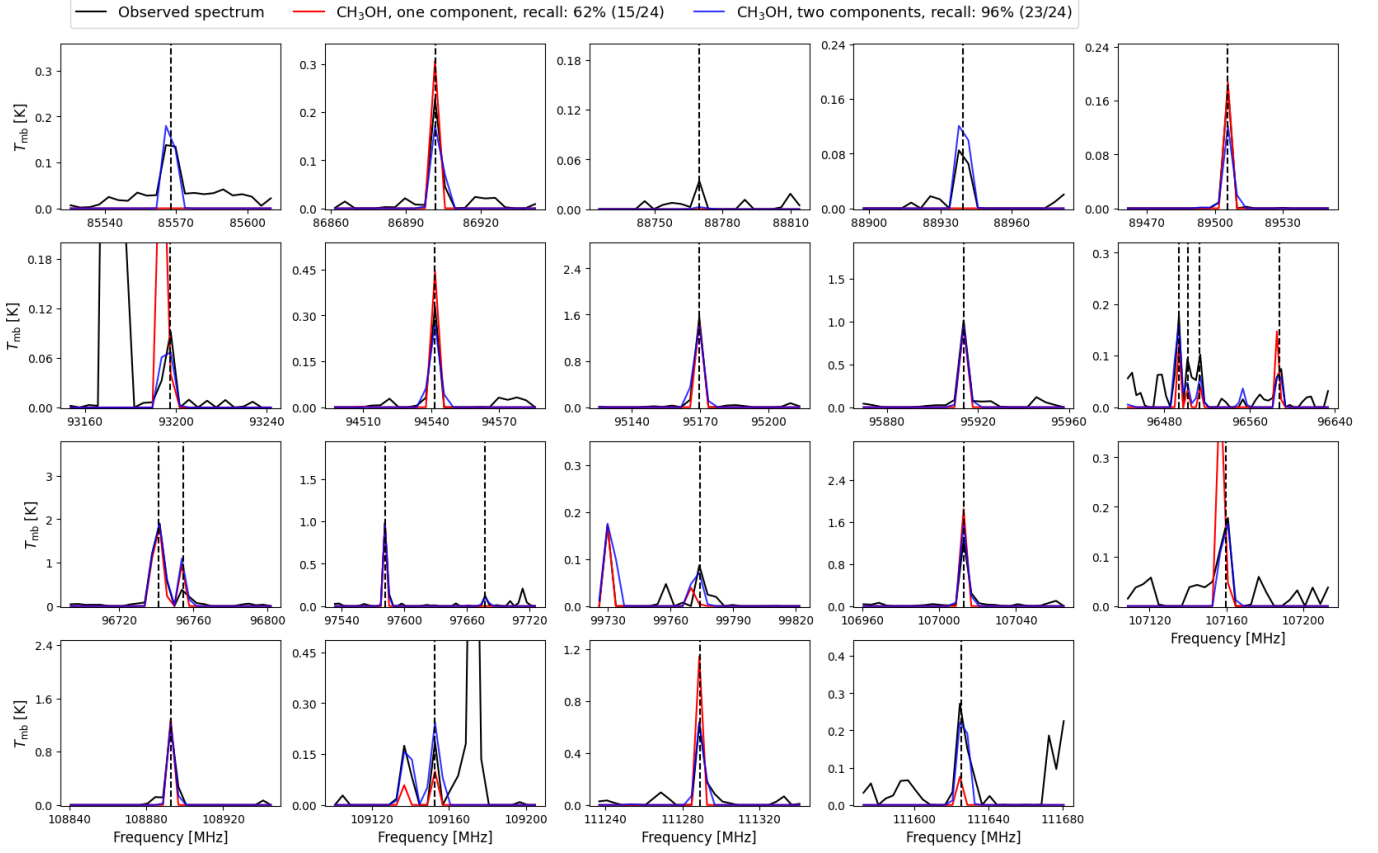


Figure 7. Spectral lines of methanol in *W51-Mopra*. Black solid lines show the observed spectrum from Watanabe et al. (2017), and black vertical lines are spectral lines of methanol identified by Watanabe et al. (2017). Red and blue lines show the fitting results using one and two physical components respectively. The recall of each fitting result is indicated in the first panel. These plots imply that the spectrum of methanol can be better modeled using two physical components.

Müller, H. S. P., Thorwirth, S., Roth, D. A., & Winnewisser, G. 2001, A&A, 370, L49, doi: [10.1051/0004-6361:20010367](https://doi.org/10.1051/0004-6361:20010367)

pandas development team, T. 2020, pandas-dev/pandas: Pandas, latest, Zenodo, doi: [10.5281/zenodo.3509134](https://doi.org/10.5281/zenodo.3509134)

Pickett, H. M., Poynter, R. L., Cohen, E. A., et al. 1998, JQSRT, 60, 883, doi: [10.1016/S0022-4073\(98\)00091-0](https://doi.org/10.1016/S0022-4073(98)00091-0)

Qiu, Y., Kang, X., & Luo, Y. 2023, MNRAS, 519, 2268, doi: [10.1093/mnras/stac3661](https://doi.org/10.1093/mnras/stac3661)

Ruiz, A. N., Cora, S. A., Padilla, N. D., et al. 2015, ApJ, 801, 139, doi: [10.1088/0004-637X/801/2/139](https://doi.org/10.1088/0004-637X/801/2/139)

Shi, Y., & Eberhart, R. 1998, in 1998 IEEE International Conference on Evolutionary Computation Proceedings. IEEE World Congress on Computational Intelligence (Cat. No.98TH8360), 69–73, doi: [10.1109/ICEC.1998.699146](https://doi.org/10.1109/ICEC.1998.699146)

Vastel, C., Bottinelli, S., Caux, E., Glorian, J. M., & Boiziot, M. 2015, in SF2A-2015: Proceedings of the Annual meeting of the French Society of Astronomy and Astrophysics, 313–316

Virtanen, P., Gommers, R., Oliphant, T. E., et al. 2020, Nature Methods, 17, 261, doi: [10.1038/s41592-019-0686-2](https://doi.org/10.1038/s41592-019-0686-2)

Wang, D., Tan, D., & Liu, L. 2018, Soft computing, 22, 387

Wang, Y., Mohanty, S. D., & Jenet, F. A. 2014, ApJ, 795, 96, doi: [10.1088/0004-637X/795/1/96](https://doi.org/10.1088/0004-637X/795/1/96)

Watanabe, Y., Nishimura, Y., Harada, N., et al. 2017, ApJ, 845, 116, doi: [10.3847/1538-4357/aa7ece](https://doi.org/10.3847/1538-4357/aa7ece)

Wes McKinney. 2010, in Proceedings of the 9th Python in Science Conference, ed. Stéfan van der Walt & Jarrod Millman, 56 – 61, doi: [10.25080/Majora-92bf1922-00a](https://doi.org/10.25080/Majora-92bf1922-00a)

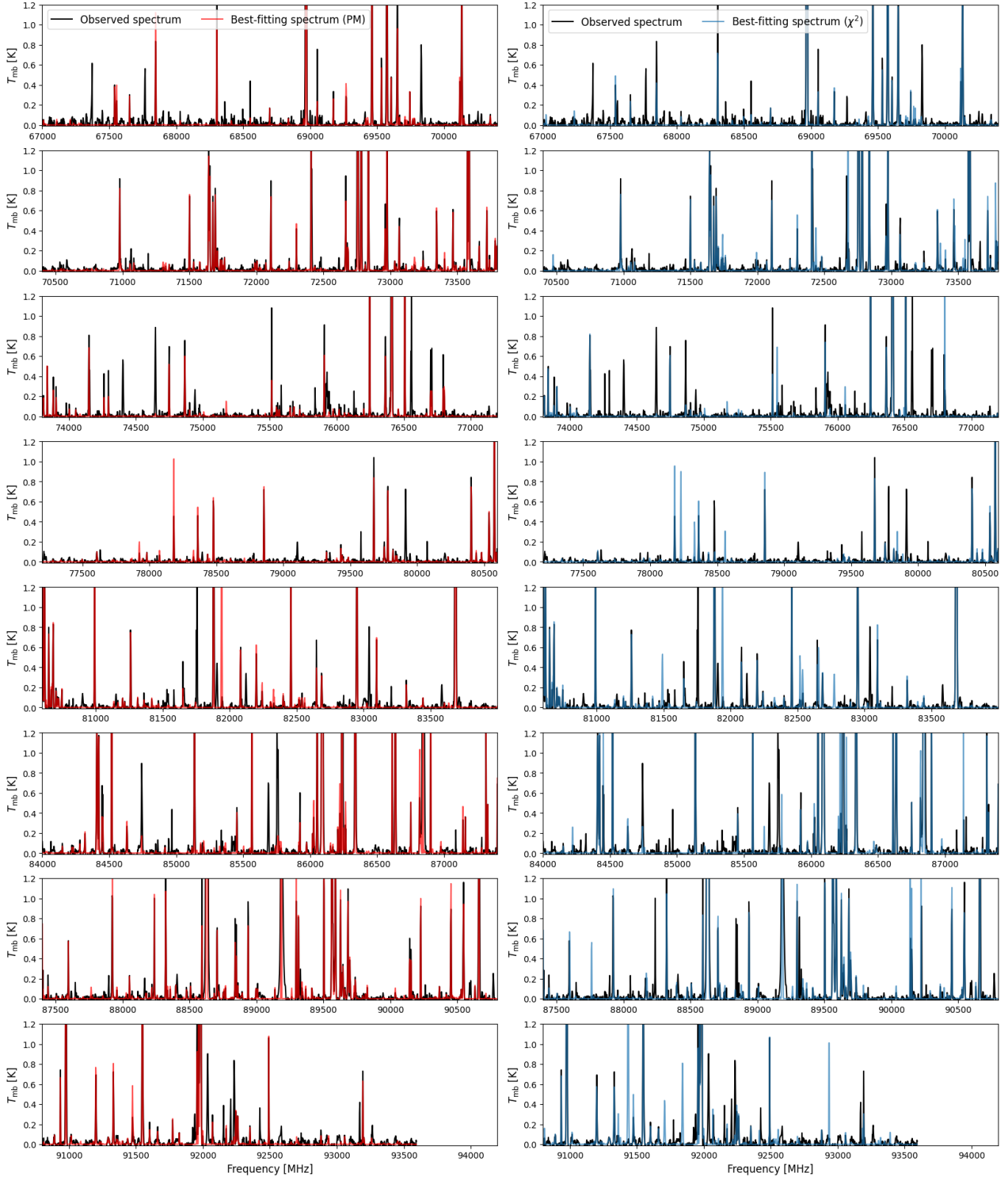


Figure 8. Best fitting results for *OrionKL-GBT*. Black lines represent the observed spectrum. Left and right panels show the results using the peak matching and χ^2 loss functions respectively. The peak matching loss function is described in Section 2.4.

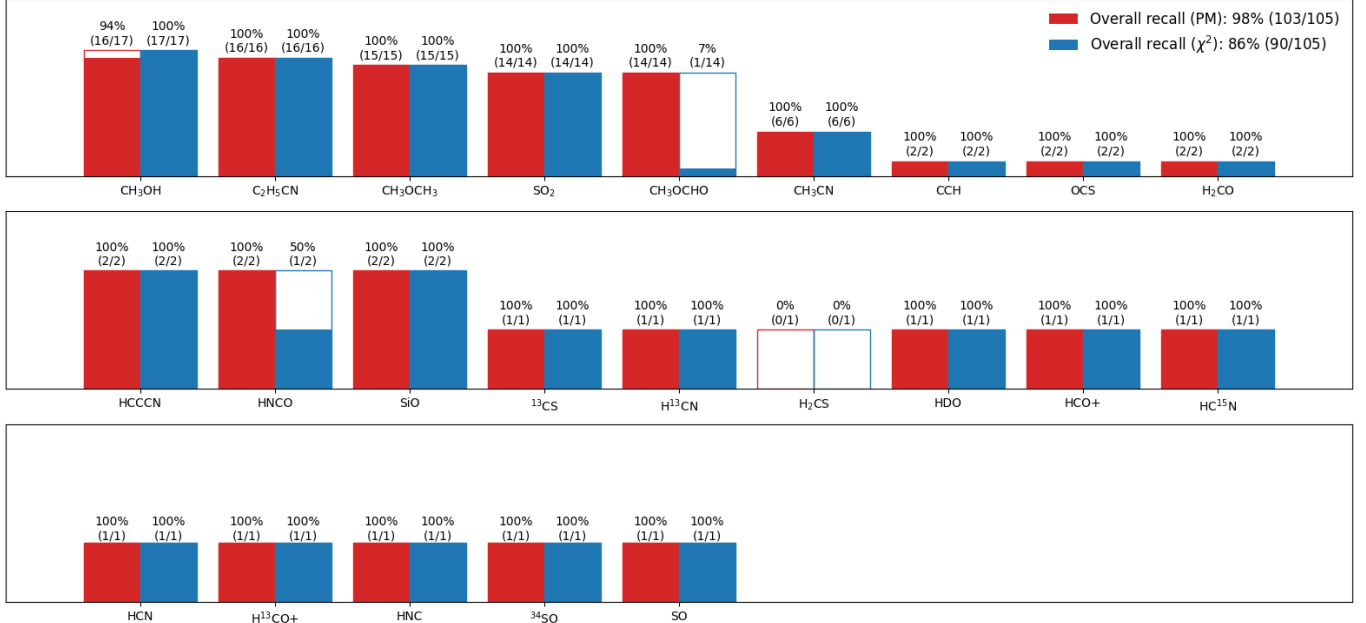


Figure 9. Recall of molecules identified in *OrionKL-GBT*. Red and blue bars illustrate the results using the peak matching and χ^2 loss functions respectively. The recall, the number of matched lines, and the number of relevant lines are indicated on top of each bar. Refer to Section 4.1 for the definition of recall.

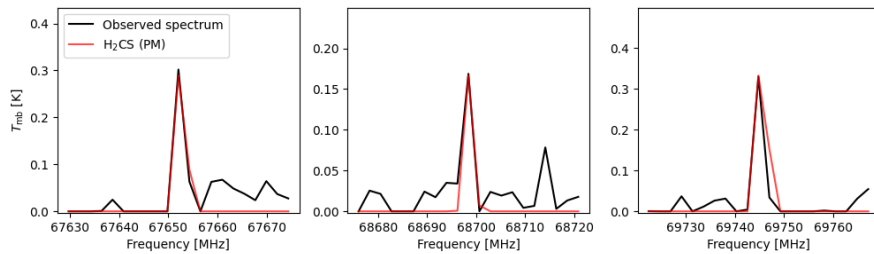


Figure 10. Identified lines of H₂CS in *OrionKL-GBT*. The result is obtained using the peak matching loss function. The result implies a different component of H₂CS in addition to the one identified by Frayer et al. (2015).

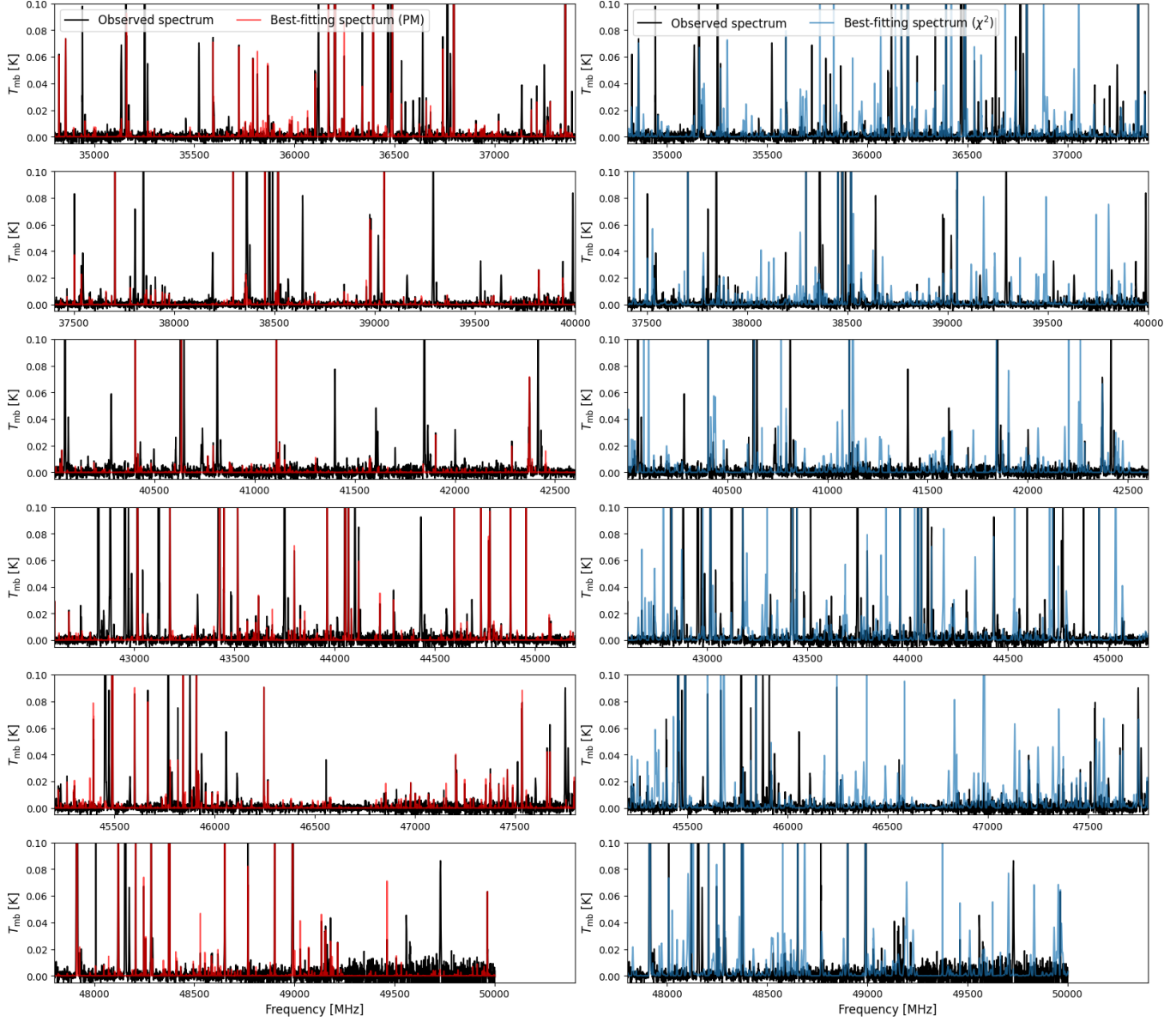


Figure 11. Best fitting results for *OrionKL-Tianma*. Black lines represent the observed spectrum. Left and right panels show the results using the peak matching and χ^2 loss functions respectively. The line survey data are introduced in Section 3.3. The peak matching loss function is described in Section 2.4.

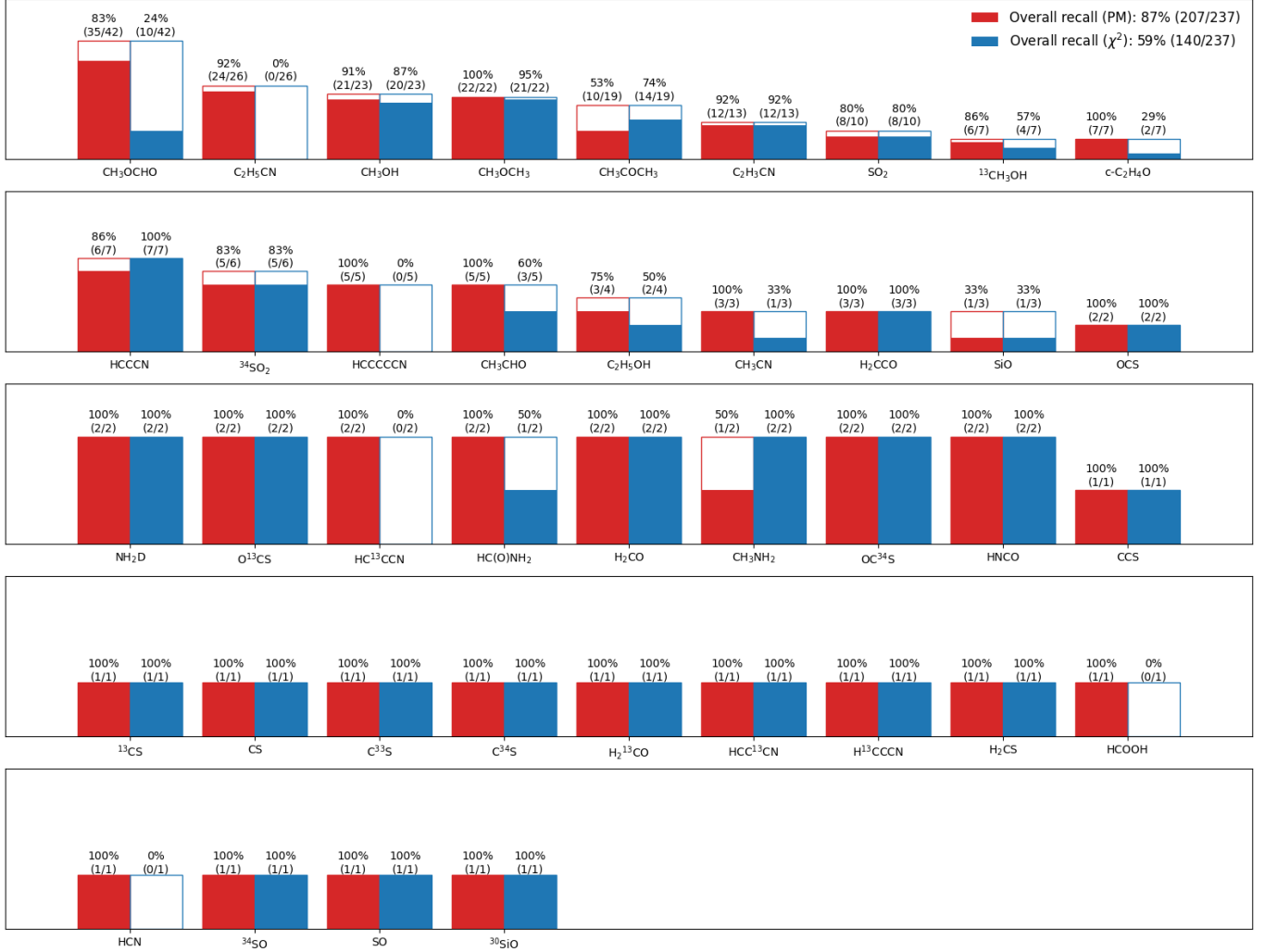


Figure 12. Recall of molecules identified in *OrionKL-Tianma*. Red and blue bars illustrate the results using the peak matching and χ^2 loss functions respectively. The recall, the number of matched lines, and the number of relevant lines are indicated on top of each bar. Refer to Section 4.1 for the definition of recall.

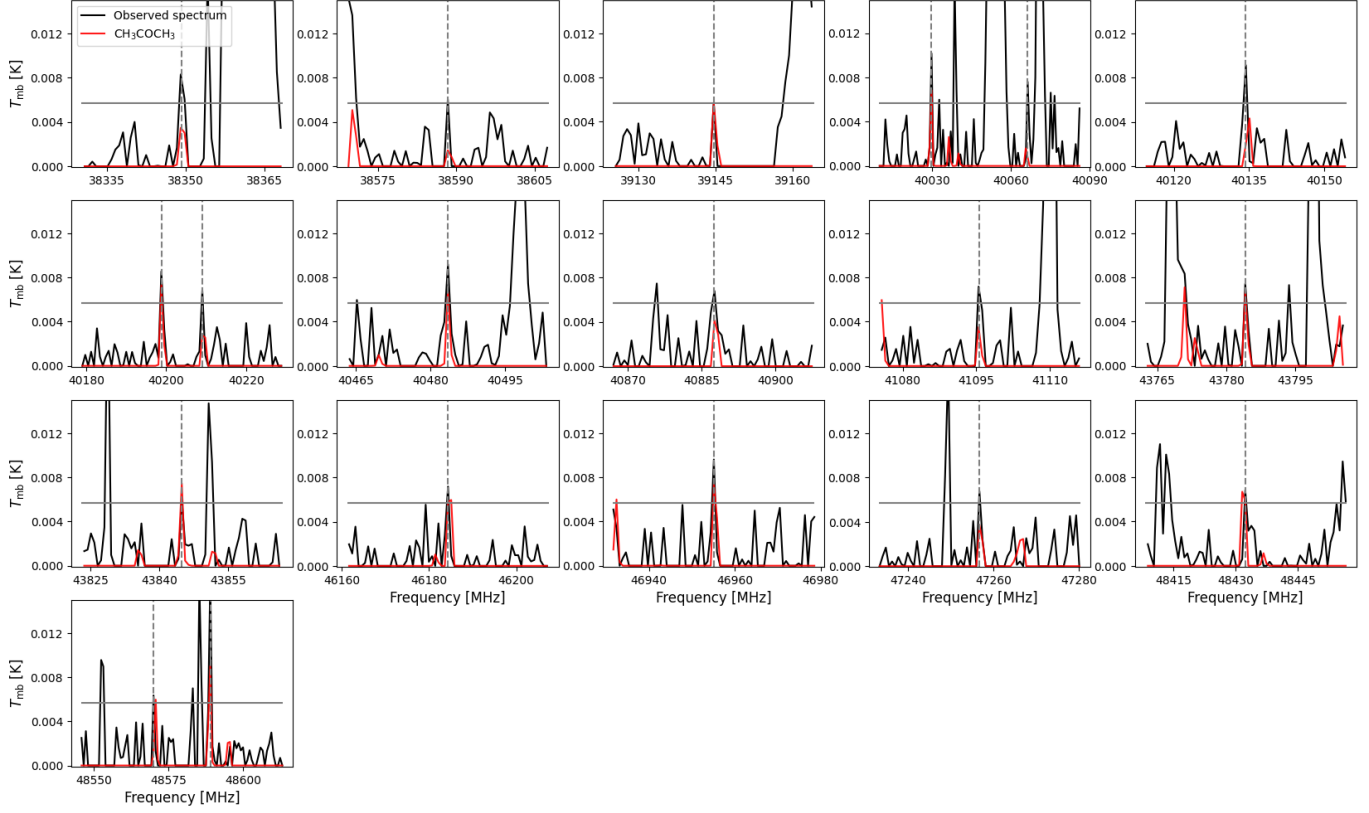


Figure 13. Line identification of acetone (CH_3COCH_3) in *OrionKL-Tianma*. Black solid lines show the observed spectrum. Black dashed lines indicate the CH_3COCH_3 spectral lines identified by Liu et al. (2022). Grey horizontal lines represent the threshold used by our algorithm to identify a peak. Red lines show the best-fitting spectrum using the peak matching loss. While the best-fitting spectrum predicts most peaks at the identified lines of Liu et al. (2022), some peaks are too faint to be identified by our peak finder. This explains the low recall of CH_3COCH_3 , as shown in Figure 12.

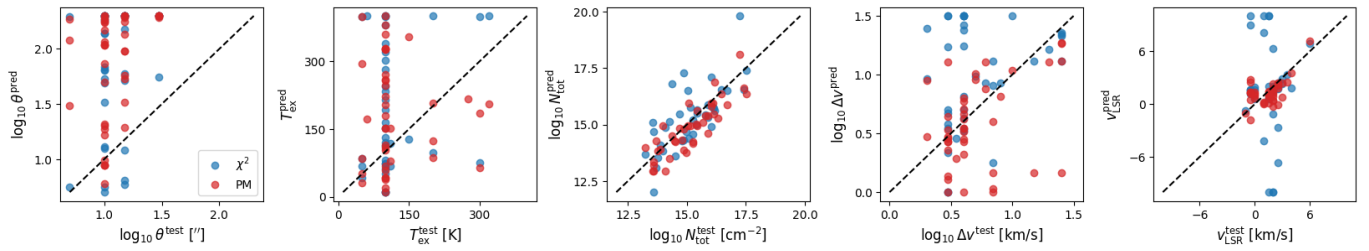


Figure 14. Comparison of the parameters estimated by Liu et al. (2022), labeled "test", with the best-fitting parameters derived from the peak match loss function, labeled "pred". Whenever the original study suggests multiple components, the component with the highest column density is compared. Red and blue dots represent the results based on the peak matching and χ^2 loss functions respectively. Each data point compares the parameters of a molecule at one state. Liu et al. (2022) adopted fixed values for source size and excitation temperature, and fit the column density, velocity width, and velocity offset.

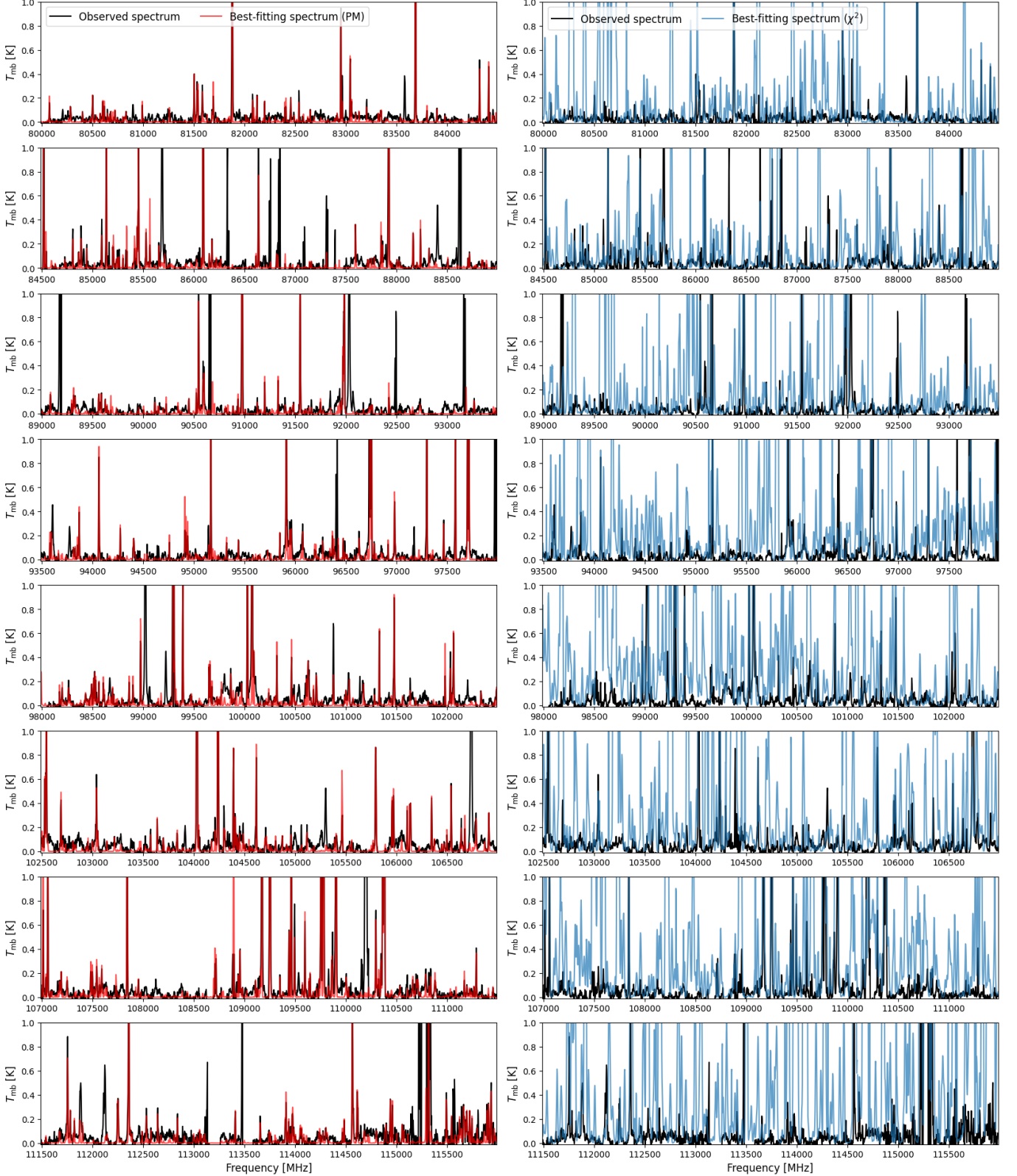


Figure 15. Best fitting results for *SgrB2M-IRAM*. Black lines represent the observed spectrum. Left and right panels show the results using the peak matching and χ^2 loss functions respectively. The peak matching loss function is described in Section 2.4.

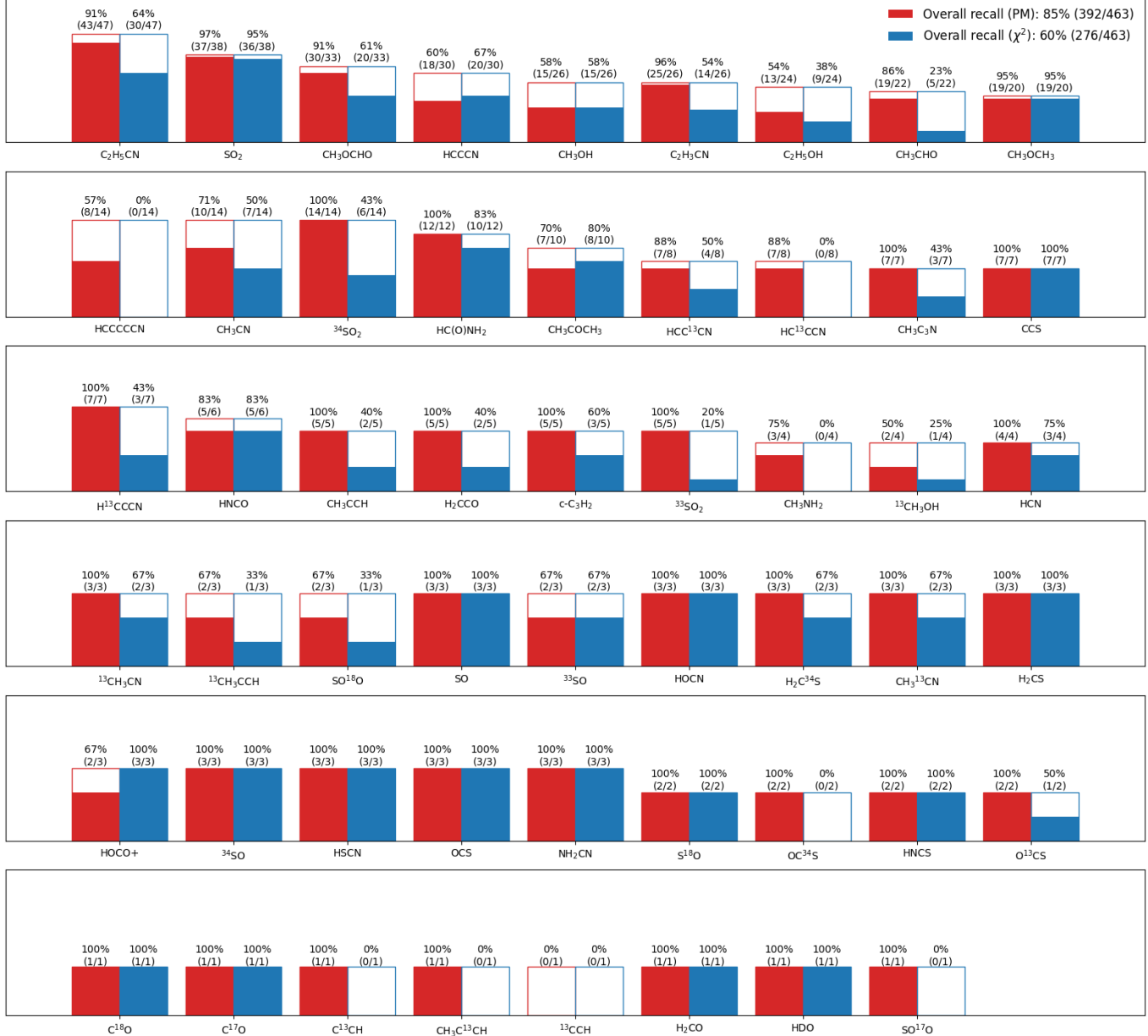


Figure 16. Recall of molecules identified in *SgrB2M-IRAM*. Red and blue bars illustrate the results using the peak matching and χ^2 loss functions respectively. The recall, the number of matched lines, and the number of relevant lines are indicated on top of each bar. Refer to Section 4.1 for the definition of recall.

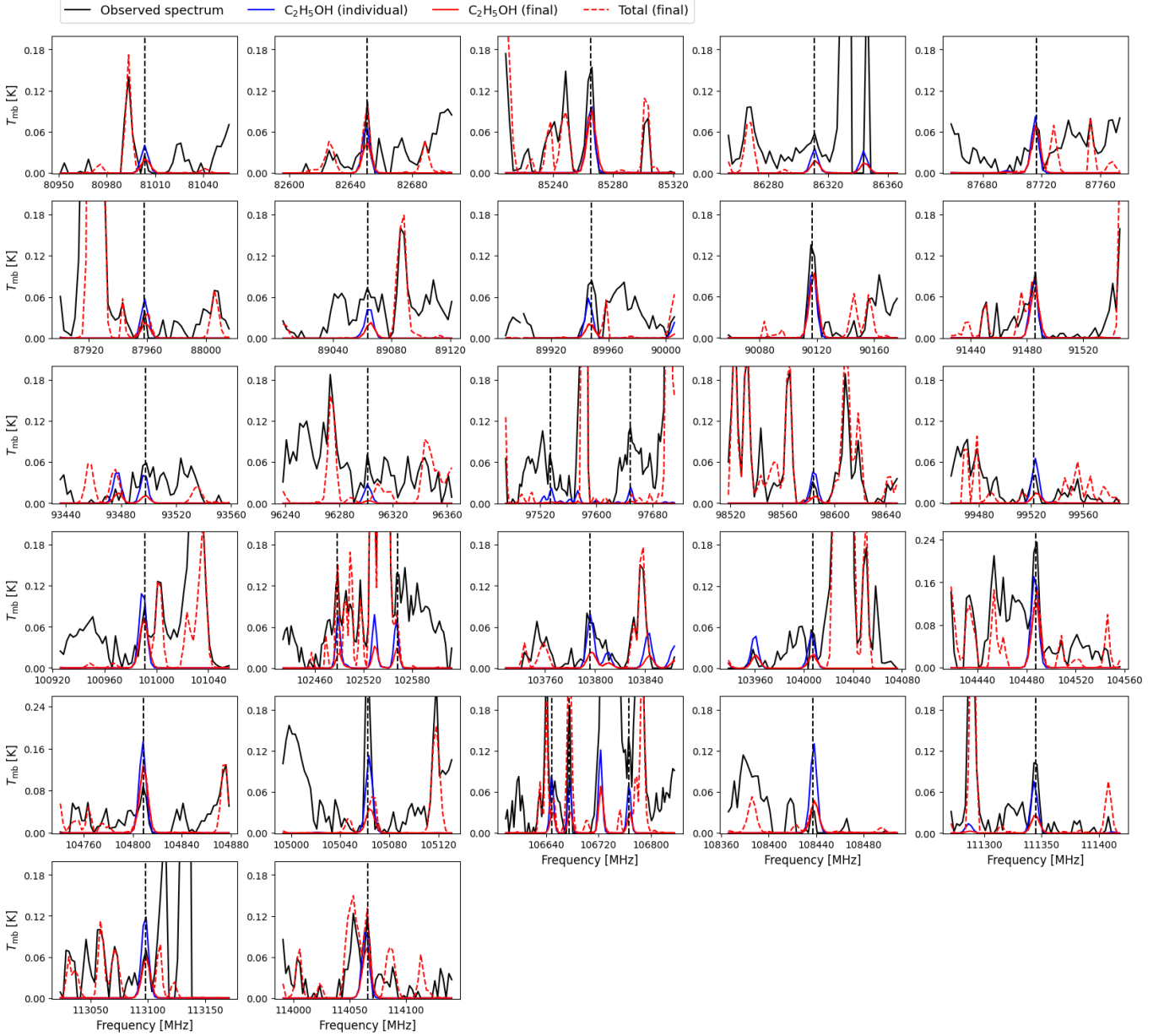


Figure 17. Line blending analysis of ethanol ($\text{C}_2\text{H}_5\text{OH}$) in *SgrB2M-IRAM*. Black solid lines represent the observed spectrum, and black dashed lines indicate the $\text{C}_2\text{H}_5\text{OH}$ spectral lines identified by Belloche et al. (2013). Blue lines show the best-fitting spectrum of $\text{C}_2\text{H}_5\text{OH}$ obtained in the individual fitting phase. Red solid lines illustrate the spectrum of $\text{C}_2\text{H}_5\text{OH}$ as a part of the combined spectrum. The final combined spectrum is shown as red dashed lines. While the final result show a low recall of $\text{C}_2\text{H}_5\text{OH}$, most lines can be recovered in the individual fitting phase, implying line blending.

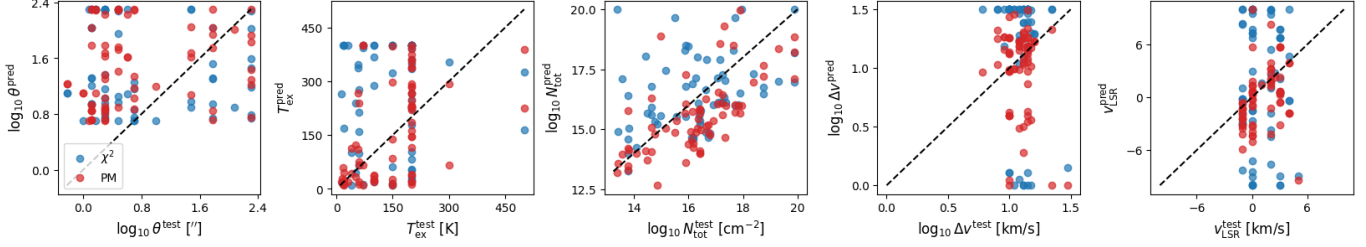


Figure 18. Comparison of the parameters estimated by Belloche et al. (2013), labeled "test", with the best-fitting parameters obtained in this work, labeled "pred". Whenever the original study suggests multiple components, the component with the highest column density is compared. Each data point compares the parameters of a molecule at one state. Red and blue dots represent the results based on the peak matching and χ^2 loss functions respectively.

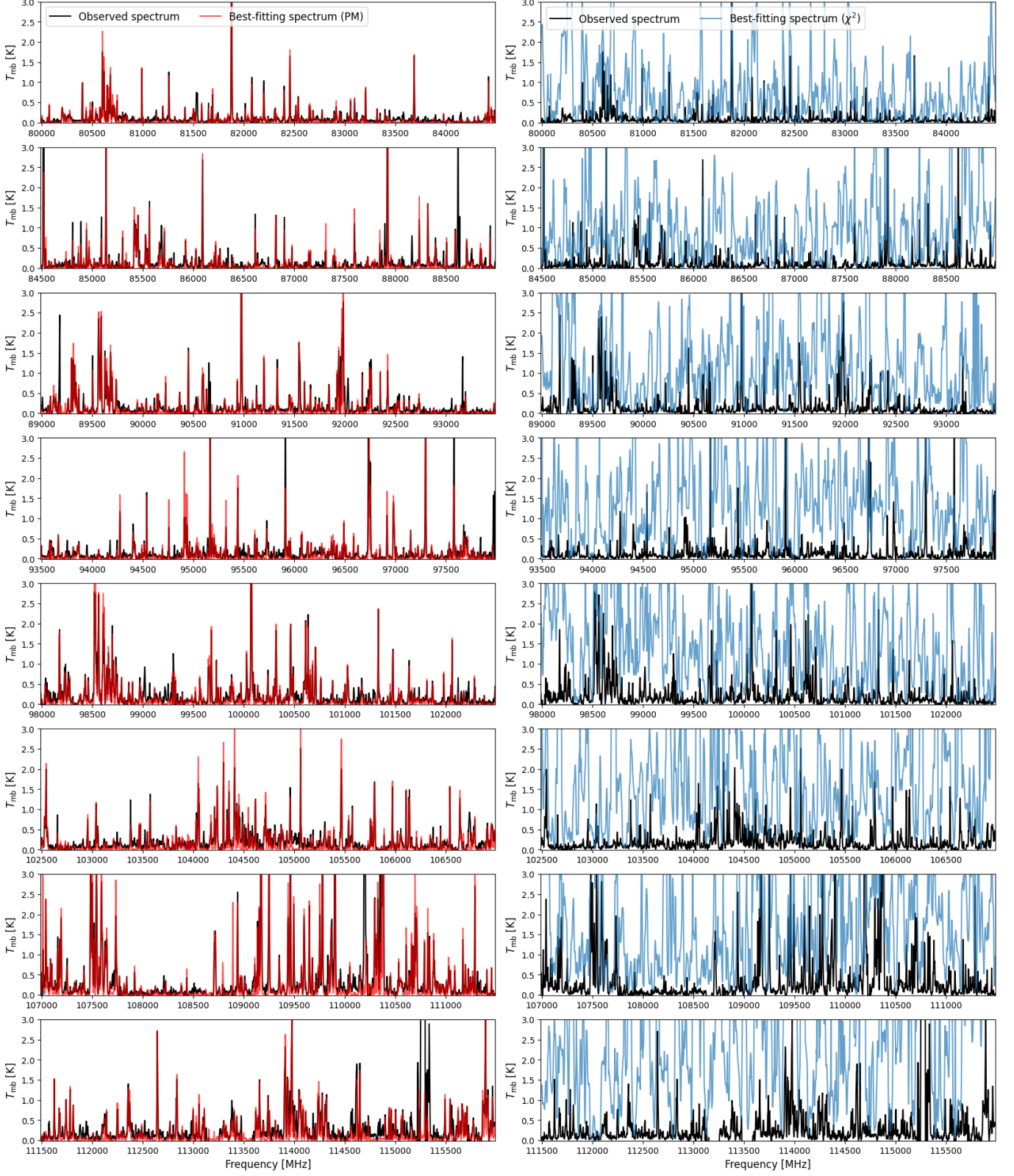


Figure 19. Best fitting results for *SgrB2N-IRAM*. Black lines represent the observed spectrum. Left and right panels show the results using the peak matching and χ^2 loss functions respectively. The peak matching loss function is described in Section 2.4.



Figure 20. Recall of molecules identified in *SgrB2N-IRAM*. Red and blue bars illustrate the results using the peak matching and χ^2 loss functions respectively. The recall, the number of matched lines, and the number of relevant lines are indicated on top of each bar. Refer to Section 4.1 for the definition of recall.

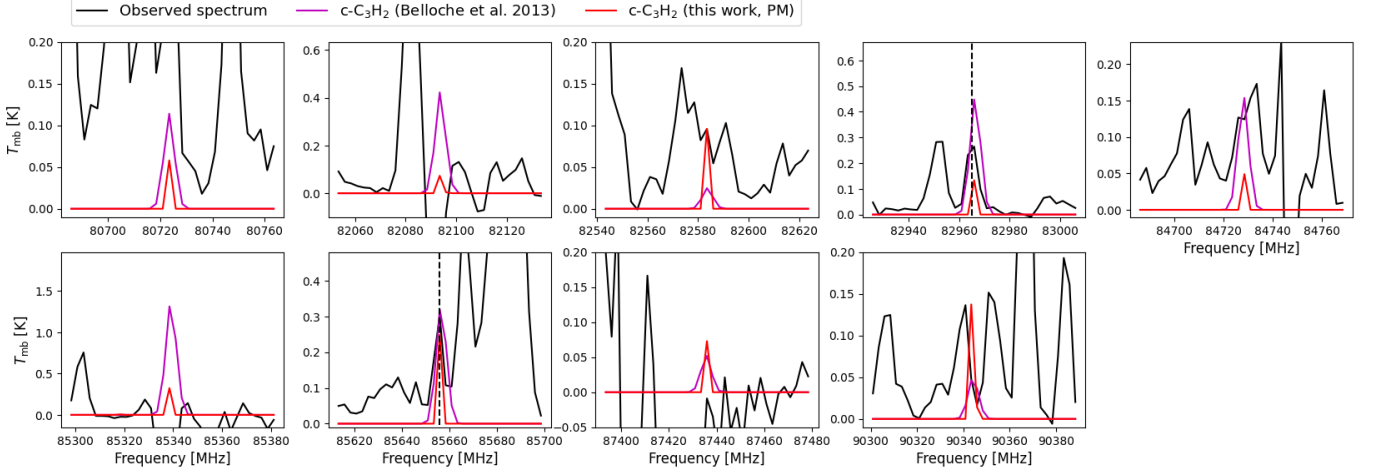


Figure 21. Line identification of cyclopropenylidene (c-C₃H₂) by Belloche et al. (2013). Black solid lines represent the observed spectrum, and black dashed lines indicate the spectral lines of c-C₃H₂ identified by Belloche et al. (2013). Purple lines represent the spectrum generated using the parameters suggested by Belloche et al. (2013). Each panel displays a peak from the model spectrum.

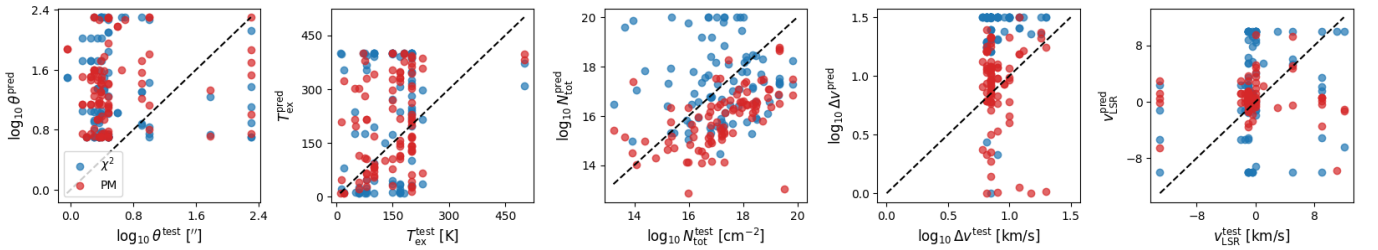


Figure 22. Comparison of the parameters estimated by Belloche et al. (2013), labeled "test", with the best-fitting parameters obtained in this work, labeled "pred". Whenever the original study suggests multiple components, the component with the highest column density is compared. Each data point compares the parameters of a molecule at one state. Red and blue dots represent the results based on the peak matching and χ^2 loss functions respectively.